Clinical Biomechanics 33 (2016) 66–72

Contents lists available at ScienceDirect

Clinical Biomechanics

journal homepage: www.elsevier.com/locate/clinbiomech

Differential displacement of soft tissue layers from manual therapy loading

Shawn Engell [a], John J. Triano [a,b,*], James R. Fox [c], Helene M. Langevin [c,d], Elisa E. Konofagou [e]

[a] Rehabilitation Science, McMaster University, Hamilton, Ontario, Canada
[b] Graduate Education and Research, Canadian Memorial Chiropractic College, Toronto, Ontario, Canada
[c] Department of Neurological Sciences, College of Medicine, University of Vermont, Burlington, VT, USA
[d] Osher Center for Integrative Medicine, Harvard Medical School and Brigham and Women's Hospital, Boston, MA, USA
[e] Biomedical Engineering and Radiology, Columbia University, New York, NY, USA

ARTICLE INFO

Article history:
Received 21 September 2015
Accepted 17 February 2016

Keywords:
Spinal manipulation
Biomechanics
Elastography
Cumulative displacement
Shear displacement
Electromyography

ABSTRACT

Background: Understanding the biomechanics of spinal manipulative therapy requires knowing how loads are transmitted to deeper structures. This investigation monitored displacement at sequential depths in thoracic paraspinal tissues parallel with surface load directions.
Methods: Participants were prone and a typical preload maneuver was applied to thoracic tissues. Ultrasound speckle tracking synchronously monitored displacement and shear deformation of tissue layers in a region of interest adjacent to load application to a depth of 4 cm. Cumulative and shearing displacements along with myoelectric activity were quantitatively estimated adjacent to loading site.
Findings: The cephalocaudal cumulative displacement in layers parallel to the surface were, in order of depth, 1.27 (SD = 0.03), 1.18 (SD = 0.02), and 1.06 (SD = 0.01) mm ($P < 0.000$), respectively. The superficial/intermediate shear was 2.1 ± 2.3% whereas the intermediate/deep shear was 4.4% (SE = 3.7, $P = 0.014$). Correlation of tissue layers was stronger with application site displacement at the surface ($0.87 < r < 0.89$) than with muscle activation ($0.65 < r < 0.67$).
Interpretation: Surface loading of the torso in combined posteroanterior and caudocephalic directions result in both displacement of tissues anteriorly and in shearing between tissue layers in the plane of the tissues strata to depths that could plausibly affect spinal tissues. Displacements of tissues more likely arise passively, consistent with load transmitted by the retinacula cutis and epimuscular force pathways. Displacements are similar in magnitude to those known to evoke biologically relevant responses in both animal and human studies.

1. Introduction

Typically, high-velocity, low-amplitude (HVLA) spinal manipulative procedures are applied to the body surface using a ramped increase in load, termed the preload phase, followed by a single impulse load designed to influence the underlying spinal joint. Different intensities (Snodgrass et al., 2014) and rates (Cleland et al., 2009) of manual loading appear to have stronger clinical effects than others. It is not yet clear how these differences propagate through the tissues and are modulated. A complete understanding of the biomechanics of manipulative therapy requires knowing the manner in which loads are transmitted between the surface application site and the deeper tissue layers and bone (Pickar, 2002). The differential response among the tissue layers may supply clues to mechanotransduction triggers and the ability to systematically modulate effects. Indeed, the whole question on whether loads are transmitted through the tissues in any controlled way to suggest a feasibility of dosing effects is a matter of controversy. The administration of loading parameters can be systematically controlled (Descarreaux et al., 2005; Descarreaux and Dugas, 2010, Triano et al., 2004, 2011, 2012, 2014, 2015), but how the soft tissues attenuate, absorb or redistribute those loads is not clear. Bereznick et al. (2002) as well as Kawchuk and Perle (2009) have measured the difference between applied load components and transmitted loads in human and porcine models, respectively. They postulate that therapeutic procedures may contain a significant component of "wasted energy" as a result of low friction coefficients between tissue layers (Bereznick et al., 2002), perhaps further constrained by the motion segment geometry (Kawchuk and Perle, 2009). Both studies suggest that little more than a tissue compression effect is transmitted posteroanteriorly.

Our goal was to directly monitor both posteroanterior and caudocephalic motion of tissue in strata at sequential depths between the load application site and targeted spinal segment in the paraspinal thoracic region. Using relative tissue displacement measured by

* Corresponding author at: Graduate Education and Research Program, Canadian Memorial Chiropractic College, 6100 Leslie Street, Toronto, Ontario, Canada M2H 3J1.
E-mail address: Jtriano@cmcc.ca (J.J. Triano).

http://dx.doi.org/10.1016/j.clinbiomech.2016.02.011
0268-0033/

ultrasound elastography as a surrogate for evidence of load transmission. We hypothesized that an HVLA preload maneuver would result in a superficial to deep sequential engaging of tissues underlying the skin. The preload phase was selected because of its known superficial tissue displacement behavior (Bereznick et al., 2002; Kawchuk and Perle, 2009) and ability to influence physiologic responses to treatment (Nougarou et al., 2014) but absent the highly dynamic elements of the impulse phase. Data of this type will help clarify how therapeutic loads interact with tissues to transfer effects through them. Such understanding will contribute to future work seeking to optimize treatment outcomes for patients receiving manipulative procedures in managing their pain and functional impairment.

2. Methods

A pre-post test experimental study design was used to evaluate the motion of subcutaneous tissue layers during the application of manual preload forces to the thoracic region of healthy volunteers. Ultrasound speckle tracking techniques (Konofagou and Ophir, 1998; Langevin et al., 2011; Ophir et al., 1991) were used to monitor the displacement and shear deformation of the paraspinal soft tissues as the primary outcomes of the study. A number of biomechanical measures were monitored simultaneously to define the experimental environment including forces transmitted through the thorax, displacement of the application hand and torso, as a rigid body, and the ultrasound sensor.

2.1. Participants

Twenty-four healthy male volunteers between the ages of 23 and 45 years were recruited from the population at the Canadian Memorial Chiropractic College (CMCC). Healthy subjects were selected for this study of mechanical effects on tissues to avoid variations due to any pathologic anomaly (Langevin et al., 2009). To control for any potential confounding effects from the presence of variable body fat depth, males with a mesomorphic body type, based on observation, were recruited (Kawchuk et al., 2011). All participants provided written informed consent that was approved by both the McMaster University Ethics (#12-594) and the CMCC Research Ethics (#122027) review boards.

2.2. Experimentation

Data were recorded from each participant during a single testing session. Prior to data capture, anthropometric data were obtained. The subject then laid prone on a treatment table (Leander LT 900, Leander Healthcare Technologies, Lawrence, KA, USA) that was modified with an embedded AMTI force plate (Advanced Medical Technology Inc., Model; OR6-7, Watertown, MA, USA) located beneath the thoracic torso support surface (Triano et al., 2012). Each subject was positioned with a standard alignment of the L4/L5 intervertebral disc at the caudal edge of the thoracic support (Fig. 1). The participant's arms were positioned at the side and internally rotated below the elbow. The inferior angles of the scapulae were identified as consistent landmarks between subjects. An acrylic block (2 cm thick × 4 cm wide × 4 cm long) was adhered to the skin overlying the erector spinae and centered approximately 2 cm left and 2 cm superior to the spinous process at the level of the left scapula's inferior angle using commercial double-sided tape to provide a uniform surface for distributing the manually applied force to the underlying tissues. The block was machined to fit a 6 degrees of freedom force transducer (ATI industrial automation, F/T model; mini 45E, Apex, NC, USA) for recording the applied forces and moments. The initial orientation angle of the block with respect to the horizontal was measured with an inclinometer to the nearest degree and, based on preliminary testing, was assumed to remain unchanged throughout the experimental maneuver. Activity of the underlying thoracic paraspinal muscle was monitored by a pair of Ag-AgCl electrodes (Biopac Systems Inc., Goleta, CA, USA), separated by a center-to-center inter-electrode distance of approximately 3 cm, that were adhered to the skin. Placement was arranged to record directly caudal to the loading site at approximately the T7 segment (Cramer and Darby, 2005). Electrodes were covered with Opsite tape (Smith and Nephew, Mississauga, ON, Canada) to insulate them from the ultrasound gel. An ultrasound transducer (Sonix RP, Burnaby, BC, Canada) was positioned medial to the electrodes, aligned parasagittally, approximately 2 cm left of the spine's midline (Langevin et al., 2009, 2011) and held in position by an independent, floor-mounted clamping system. The recording locations, as described, limited the characterization of behavior to those tissues caudal to the application site.

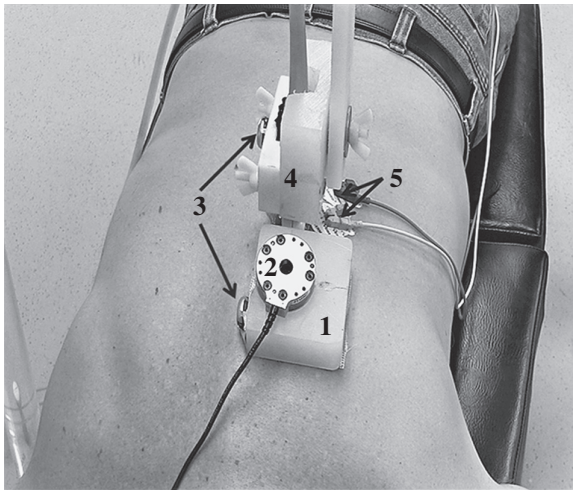

Fig. 1. Data capture configuration showing (1) the preload application block, (2) the ATI load cell, (3) infrared diode markers, and (4) clamped ultrasound transducer. An additional right acromion diode marker is not shown.

In the parasagittal plane, two ultrasound recording sites were identified. The first (proximate) site was located directly caudal to the loading block. The second region (distant site) was also 2 cm lateral to the midline and caudal to the proximate site. The caudal location was standardized as one-third of the distance from the load application site to L5/S1.

A single optoelectronic camera (Optotrak Certus System, Northern Digital Inc., Waterloo, ON, Canada) was positioned 2.5 m to the side of the participant. Infrared-emitting diode markers were placed in three locations to monitor relative body segment displacements. One marker was affixed to the acrylic block through which loads were applied. A second was positioned on the ultrasound head while the third was placed over the subject's right acromion process to monitor any concurrent torso displacement during the experimental maneuver.

2.2.1. Experimental maneuver

Two experimental maneuvers were performed sequentially, first with the ultrasound recording at the proximate site and secondly with it at the distant site. All data capture was time-synchronized based on an independent signal triggered by initiating the ultrasound capture. After sonation began, a clinician with 6 years of experience in manual therapy applied force to the subject through the load cell and acrylic block. The force modeled the typical “preload” phase that is designed to induce tension in the underlying tissues before a high-velocity and low-amplitude (HVLA) thrust would be applied. The direction of force was caudocephalic and secondarily posteroanterior with respect to the subject's torso. During the maneuver, the block was allowed to displace cephalad (Fig. 2) until the clinician perceived maximal resistance to tissue movement. The total time for the experimental maneuver was less than 10 s.

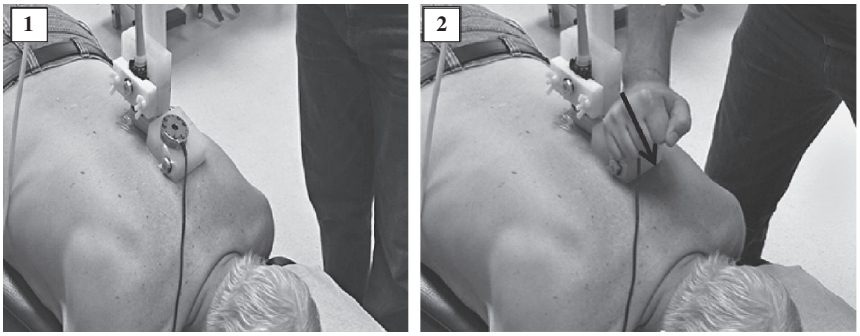

Fig. 2. The instrumentation setup (1) showing the clamp holding the ultrasound transducer and sensor for monitoring the input load to the subject. The experimental maneuver (2) consisted of force applied posteroanteriorly and caudocephalically. The muscle recording surface electrodes are obscured behind the ultrasound.

2.3. Data capture parameters and ultrasound data reduction

All kinematic data were recorded with a 64 Hz sample rate. Applied and transmitted forces and moments as well as the myoelectric activity of the paraspinal muscles were sampled at 2048 Hz. The ultrasound image field depth was set at 40 mm with 50% sectoring of the 38 mm linear array transducer, effectively reducing the windowed tissue to 19 mm in a caudocephalic, parasagittal plane. Tissue images were sampled at 51 Hz with a 40 MHz interrogation signal and 10 MHz receiving mode. The focus of the ultrasound beam was placed at the mid-intermediate layer. Both cine-loop B-mode images and radiofrequency (RF) signals were stored over the full 10-s testing interval. The ultrasound also provided a time synchronization pulse that was captured along with the kinematic, kinetic and myoelectric data through a 16-channel Optotrak™ digital acquisition unit (Northern Digital Inc., Waterloo, ON, Canada).

2.4. Data reduction and post-processing

Signal post-processing for all of the data was managed through Matlab ™ (MathWorks, Natick, MA, USA). The synchronized kinematic, kinetic, and ultrasound data were digitally re-sampled to match the USN data prior to further post-processing due to the incongruence between sample rates for each modality. To accomplish this task, the test maneuver was isolated by windowing the time-linked data based on the start and stop pulses from the ultrasound synchronization. Fig. 3 displays a typical set of kinematic data for markers moving in the caudocephalic direction. The start of force application was identified by marking the inception of displacement for the marker affixed to the acrylic block. The interval terminated when the displacement reached a stable maximum plateau. Kinematic and load data were digitally filtered using a dual-pass 2nd-order Butterworth filter with a 4 Hz cutoff frequency. Myoelectric signals were used to define a transfer function for representing an estimate of muscle tension following the work of Brereton and McGill (1998). Raw signals were full-wave rectified, and digitally filtered with a 2nd-order Butterworth filter using a 2.5 Hz cutoff frequency and served as a surrogate for tension during data analysis.

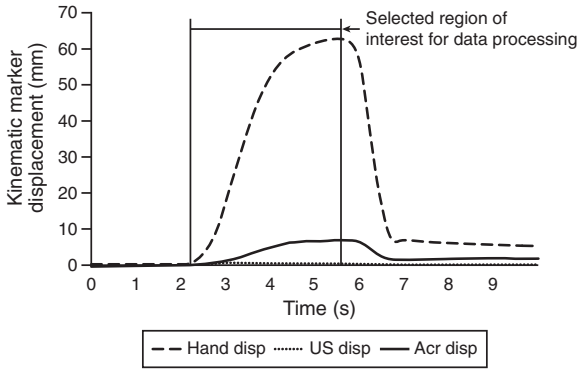

Fig. 3. Kinematic response to the experimental loading of the thoracic soft tissues in the caudocephalic direction. Displacement measures are of the loading block where force was applied (Hand), the ultrasound probe (US) and the marker on the subject's right acromion (Acr Disp) process. Vertical lines demarcate the interval region during which data was analyzed.

Quantitative reduction of the data was achieved through custom proprietary software (Courtesy of Elisa Konofagou, Columbia University) designed to process the RF signals using speckle tracking and cross-correlation techniques as validated in previous works (Konofagou and Ophir, 1998; Langevin et al., 2011; Ophir et al., 1991). The technique of speckle tracking is mathematically intensive and relies upon tissue microstructure and macrostructure RF scatterers. A brief conceptual description follows. For details, see the work of Konofagou and Ophir (1998). A standardized region of interest (ROI; 10 mm caudocephalic, 35 mm deep) was selected by placing a rectangular template subadjacent to the image boundary allowing for the transducer/skin interface artifact. For each time sample image, the location of RF scatterers was mapped. Measure of displacement was based on a weighted interpolation method operating between neighboring RF lines and comparison of cross-correlation between small rectangles of successive time sample images for a high precision tracking (Konofagou and Ophir, 1998) to quantify tissue motion in both axial and lateral directions. The location of the peak covariance estimate indicates the amount of displacement between images. The accuracy of this method has been demonstrated to be within 0.1 to 0.5 mm directly related to the strength of cross-correlation. Behavior of the tissues within the ROI was tracked throughout the experimental maneuver.

A bidirectional coordinate system was assigned for each ROI. The caudocephalic direction (e.g. "lateral" by ultrasound elastography convention) defined tissue motion in the plane of the tissues imaged within the ROI. The posteroanterior direction (e.g. "axial" by convention) defined the depth of tissue motion. Three functional layers of tissue were identified (Fig. 4) based on monitoring of the B-mode image cine-loop. The first layer was defined as being bounded by the dense fascial plane separating the subcutaneous loose connective tissue (superficial layer) from the underlying muscle. The second (intermediate) layer was functionally determined as the demarcation where the depth of muscle above appeared to undergo relatively uniform behavior but was distinct from the behavior in the third (deep) layer below. The speckle tracking algorithm provided instantaneous displacement estimates (i.e. displacement that occurred between adjacent USN frames) for each layer. Bidirectional (caudocephalic and depth) estimates were represented as an average and located at the center of each ROI layer within each frame. Layer depths and thicknesses were quantified

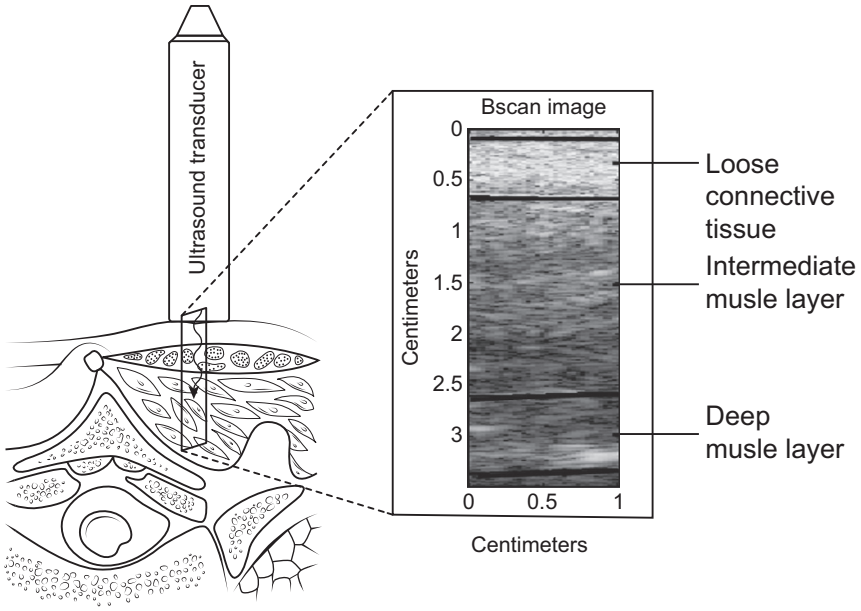

Fig. 4. Schematic cross-section scaled in context from an anatomical atlas (Koritke' and Sick, 1983) around T7 showing the ultrasound B-mode image region of interest (ROI: 10 mm × 35 mm) from which individual tissue strata were identified. Structural boundaries defined the superficial (loose connective tissue) layer while motion behavioral boundaries defined the intermediate and deep layers as described in Section 2.4.

directly from the B-mode image in millimeters for statistical descriptions of the tissue.

The dependent variables of interest were the cumulative caudocephalic displacement within each layer and the relative shear between the layers. The cumulative displacement (CD) was calculated as the integral of displacement per unit time sample over the interval of interest and expressed in millimeters (Eq. (1)).

$$CD=(1/fs)\int s_i\,dt, i=1\ \ to\ \ T;\quad \begin{array}{l} fs = \text{sampling rate},\\ s_i = \text{i}^{\text{th}}\text{displacement}/\text{i}^{\text{th}}\text{time}\end{array} \tag{1}$$

The relative shear, as movement difference between layers in percent, was determined after the work of Langevin et al. (2011) and is shown in Eq. (2).

$$S=\sum|(CD_{j+1}\text{-}CD_j)|/d;\quad \begin{array}{l} S = \text{cumulative shear},\\ j = \text{strata layer}\\ d = \text{measured separation of strata centroids}\end{array} \tag{2}$$

2.5. Data analysis

Measures of central tendency were calculated for demographic data and all dependent and independent variables using MINITAB version 15 (Minitab Inc. State College, PA, USA). Data were evaluated for normality (Anderson–Darling test), and equality of variance (Bartlett's test). For intra-rater reliability of the technician selection of layer depths, measures were repeated on 10 randomly selected subjects at a 4- to 5-month interval and tested, without reference to the original measures, by intraclass correlation coefficients. Ultrasound speckle tracking quality control was evaluated by interframe cross-correlations on the RF data.

Descriptive statistics are listed as means with standard deviations. Key variables related to the hypotheses are reported with mean and standard errors. The outcome of tissue strata cumulative displacement was the primary measure for the primary hypothesis from which all others were derived. For the intermediate and deep layers, where full data sets were available, as explained in the results, a two-way repeated measures ANOVA was performed, accounting for ultrasound recording sites and tissue layers. For the superficial layer and calculated shear between layers, paired Student *t*-tests adjusted for multiple comparisons ($\alpha = 0.0167$) were performed. Other analyses of potential explanatory variables were evaluated by Student *t*-test or, in case of non-normality, by Wilcoxon sign rank test with significance set at $\alpha = 0.05$. Associations between application site motion, myoelectric generated muscle tension and tissue layer movement were evaluated by correlational analysis.

3. Results

The primary focus of this report is on quantitative tissue behavior under the influence of the transmitted loads through the torso. The following results are grouped according to the ultrasound recording site, proximate versus distant. There were variations in the sample size for each tissue strata due to speckle tracking de-correlation between images in some cases. As a result, tissue displacement and shear data for tissue of the superficial layer at the proximate site is only available for 21 (87.5%) participants. However, data for all 24 (100%) participants is available for the second and third tissue strata. The de-correlation issues were more common for the distant site superficial layer and data is available for 10 participants (41.7%). Again, all data for deeper layers were available.

3.1. Participants

The mean age of the cohort was 25.0 (SD = 2.3) years. Their body mass index ranged from 21.8 kg/m^2 to 28.9 kg/m^2 (25.0 kg/m^2, SD = 2.0). The spinal length from load application to L5/S1 ranged from 30 to 35 cm (32.2 cm, SD = 1.7).

3.2. Force application

The initial orientation of the load application site block with respect to the horizontal in the parasagittal plane was 9.4° (SD = 4.5°), angled

toward the floor as a function of the upper thorax kyphosis. Based on preliminary study in similar subjects ($n = 10$), change of orientation angle during the experimental maneuver was considered negligible (6.9°, SD = 2.8) and not independently measured further. The travel distance of cephalad displacement for the application site was 3 mm greater (51.3, SD = 10.7 vs. 54.1, SD = 11.1 mm; $P = 0.004$) and at a rate of 60 mm/s^2 higher peak acceleration (144.7, SD = 41.7 vs. 204.1, SD = 71.8; $P = 0.001$) for the distant site. The peak transmitted forces measured at the force sensing platform, however, were comparable at 91.5 N (SD = 18.8) and 97.1 N (SD = 26.6) for the proximate and distant sites, respectively. The rate of peak force development also showed a higher trend for the distant site (32.0, SD = 8.2 vs. 37.0, SD = 11.6 N/s; $P = 0.052$). Torso displacement, as represented by the movement of the acromion marker in the cephalic direction, averaged 8.0% (4.5 mm, SD = 1.8) of the experimental maneuver when recordings at the proximate site were obtained and 9.0% (4.8 mm, SD = 2.3) for the distant site. Posteroanterior displacement was 10.4 mm (SD = 3.8) and 9.8 mm (SD = 3.3) for the proximate and distant sites respectively, reflecting compression of the thorax.

3.3. Ultrasound findings

Cross-correlation of speckle patterns, as an index of quality control for motion measurements, ranged from an average of 0.747 and standard deviation of 0.113 for the superficial layer with 0.853 (SD = 0.100) and 0.894 (SD = 0.057) for the intermediate and deep layers. The intra-rater reliability for identifying tissue layers was excellent with ICC > 0.98. Differences within repeated measures ranged from 0.16% to 0.45% of the mean layer thickness dependent upon the layer. All strata were thicker (Table 1) at the distant recording site ($P < 0.01$) consistent with the observed depth of the paraspinal musculature at more caudal locations (Chaffin and Andersson, 1984; Cramer and Darby, 2014). Layer cumulative displacements (Eq. (1)), determined by speckle tracking, were monotonically decreasing in the longitudinal caudocephalic axis parallel to the spine and in the posteroanterior axis and were consistent with the direction of load application. The superficial-to-deep cumulative displacement (d_t) was approximately uniform ($3.5 < d_t < 3.7$ mm) for all of the layers at both recording sites.

Strata cumulative displacement behaviors were similar at the proximate and distant sites (Fig. 5). That is, with increasing depth of tissue there was a sequentially decreasing rank order in the mean cumulative displacement. Each layer experienced significantly greater displacement at the proximate site (superficial layer, $n = 21$, $P = 0.003$; intermediate and deep layers, $n = 24$, $F = 14.77$, $P < 0.001$). There was also a significant overall difference in displacement between layers (superficial vs. deep) ($F = 71.27$, $P < 0.001$). The cumulative proximate site displacement means with standard error, in order of depth, were 1.27 (SE = 0.03), 1.18 (SE = 0.02), and 1.06 (SE = 0.01) mm, respectively. The distant site cumulative displacements ranked similarly at 1.14 (SE = 0.03), 1.09 (SE = 0.01), and 1.01 (SE = 0.01) mm. Fig. 6 displays the displacement-time profiles of the three different layers from which the cumulative displacements were calculated (Eq. (1)). Notice that for any instant in time, the superficial and intermediate layer instantaneous displacements are similar, while the deep site is consistently lower. Given the similarity in behavior, the remaining data descriptions will focus on the proximate site.

The calculation of relative shear between layers lumps this behavior at the center of the interface between the layered blocks defined by

Table 1
Thickness mean and standard deviation of layered strata sampled by the region of interest.

Layer (mm)	Proximate site	Distant site	P
Superficial	4.6 (2.7)	6.1 (2.7)	<0.003
Intermediate	4.2 (3.8)	7.3 (3.0)	<0.002
Deep	9.0 (5.0)	13.0 (4.0)	<0.003

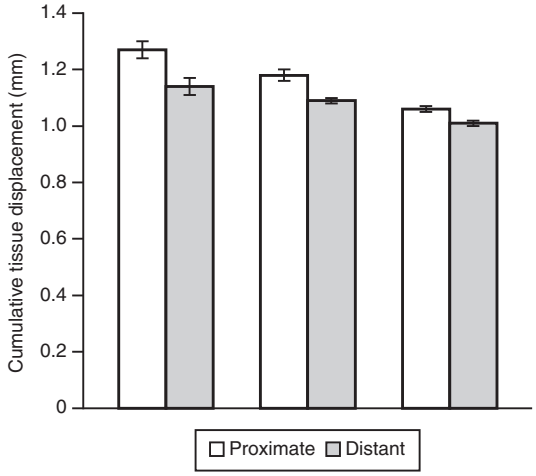

Fig. 5. Cumulative displacement of tissue strata, mean and standard error, comparing proximate and distant site recordings. Sup = superficial; Int = intermediate; Dp = deep.

Fig. 4 and Eq. (2). Represented this way, the shear incorporates both any legitimate interstitial or muscle fiber deformation, which is likely negligible for the muscle tissues (Gras et al., 2012), and the cumulative sliding between them. Inspection of the B-mode cine-loop suggests that this phenomenon is actually distributed along the depth of the tissues, as might be expected. The superficial/intermediate shear was 2.1% (SE = 2.3) whereas the intermediate/deep shear was 4.4% with standard error of 3.7 ($P = 0.014$).

Important to understanding the nature of tissue layer behavior is the correspondence of movements with any muscular contraction, either voluntary or reflexic. As seen in Fig. 6, myoelectric behavior was most frequently flat. Occasional instances of gradual ramping or bursting responses were observed. Correlations (Table 2) were performed between layer displacements and both surrogate muscle tension and loading site displacement. Lower correlations were observed with the EMG-based surrogate for muscle tension than with loading site displacement.

4. Discussion

The current investigation was the first to directly interrogate the capacity of the soft tissue structures to carry manually applied loads caudocephalically in the plane of the tissue strata to depths that could plausibly affect spinal tissues. Soft tissue displacements were paralleled

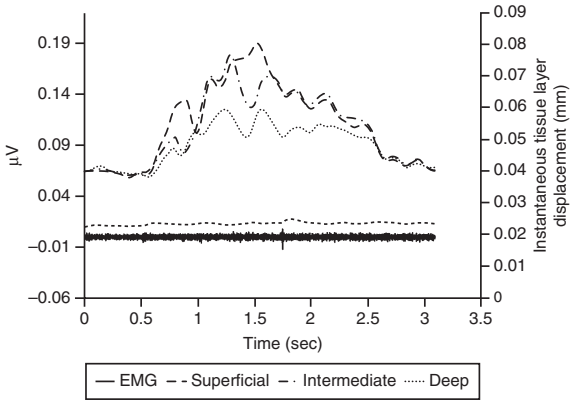

Fig. 6. Example of instantaneous displacements, in millimeters, of tissue layers from the proximate site plotted with synchronized raw myoelectric activity (μV) and filtered emg serving as surrogate for muscular tension (narrow dashed line).

Table 2
Mean correlation coefficients and probability values testing the associations between instantaneous tissue displacements and muscle tension and for load application site and cumulative tissue displacements by strata layer.

	Muscle tension	*P* value	Loading site	*P* value
Superficial	$r = 0.67$	<0.001	$r = 0.89$	<0.001
Intermediate	$r = 0.66$	<0.001	$r = 0.90$	<0.001
Deep	$r = 0.65$	<0.008	$r = 0.87$	<0.001

by the smaller acromion displacement suggesting some caudocephalic load transmission to impart movement of the torso body segment as a whole. Interestingly, the superficial loose connective tissue, a primarily passive layer, and the intermediate muscle tissue layer instantaneous displacements (Fig. 6) were nearly the same throughout the test maneuver. This implies a load transmission pathway between them comparable to the epimuscular load pathway between muscles through connective tissue structures as described by Huijing (2003); Maas and Sandercock (2010); Yucesoy (2010). In fact, the work of Nash et al. (2004) define the "retinacula cutis" as a complex of fibrous structures that traverse the subcutaneous fat linking the skin to the deep fascia and capable of transmitting loads from multi-directional forces. Together, these "skin ligaments" and the epimuscular load transmission mechanisms seem consistent with the data presented showing successive motion to depths adjacent to bone.

The effect of surface load on displacement and shear at increasing depths is non-uniform and similar to the results reported by Fox et al. (2014). They identified progressively less displacement and shear strain with increasing distance from the load application site. The relative shear from manual forces at the surface resemble the intramuscular shear from oscillation of an acupuncture needle (Fox et al., 2014), ranging from 2.2% to 5.4% dependent on the proximity to the needle. The differences in the relative shear at layer boundaries of the work reported here were comparable ranging from 2.1% at the superficial to intermediate anatomical boundary to 4.4% at the intermediate/deep functional boundary.

Most relevant is the question of whether the cumulative displacements of 1 mm observed near the bone (Fig. 4), were sufficient to suggest them as a source of biological effect. Pickar (2002) and Reed et al. (2013) have suggested the capacity of load to paraspinal tissues may be sufficient to directly stimulate receptors. Muscle spindle responses to input displacements ranging from 1 to 3 mm have been demonstrated in cats (Reed et al., 2013). Nathan and Keller (1994) intraoperatively applied a peak impulse force of 72 (SD = 9.0) N to the L2 spinous process of a subject producing 1.62 (SD = 1.06) mm peak-to-peak displacement on the caudocephalic axis. In a later study using similar methods in four patients Colloca et al. (2003), recorded paraspinal myoelectric and S1 root potentials from forces at 150 N. More recently, Nougarou et al. (2014) demonstrated that the amplitude of preload force (e.g. 5–140 N) appears to modulate reflex myoelectric response. The data of the present work further supports the idea that manually induced displacements of the tissues have potential biological impact.

Finally, it is reasonable to query whether the tissue displacements observed were a consequence of myoelectric activation. As seen in Fig. 6, the majority of cases showed little, if any, response to the experimental maneuver. Further, strong correlations were found between tissue layer cumulative displacement and surface motion at the application site. Intramuscular tension estimates, defined by the surrogate of filtered myoelectric activity, were less convincing. Tissue displacement, even at depth, appears more likely to be passively induced rather than a response to active muscle function.

5. Conclusion

Surface loading of the torso in combined posteroanterior and caudocephalic directions result in both anterior displacement of tissues and caudocephalic shearing between tissue layers in the plane of the tissues. The relative displacements and shear between layers is consistent with load transmission along the anatomical fibers of the retinacula cutis together with the deeper epimuscular connective tissue. There appears to be sufficient transmission to result in biologically relevant displacements at the depth of spinal tissues and over a breadth of several centimeters. Future work will be necessary to evaluate loads applied beyond the preload levels where tissue elasticity may be at its upper limits.

6. Limitations

The major limitation of this work is the inability to directly measure force within the tissue structures. Such effort faces both technological and ethical challenges. The instrumentation available was limited in its rate of ultrasound sampling; requiring motions at lower rates than those expected during the dynamic phase of HVLA procedures. Even at these lower rates, problems with out-of-plane motion can interfere with speckle tracking resulting in decorrelation of the signal from any given layer. The difference in application site acceleration observed between the proximate and distant recording sites may explain the higher incidence of ultrasound decorrelation in the distant superficial layer. While monitoring the between-frame cross correlations is helpful, it is likely that cumulative displacement measure as the correlations drop are underestimating the actual motions. The sole use of male subjects in this report may not be generalizable to the effects of similar loading of tissues in females. Similarly, the application of loads, proximate consistently followed by distant, may have had an influence on the tissue responses as a result of the sequencing. Finally, use of a solid block interface at the skin provided a more uniform surface for load distribution which may not reflect local maxima likely to arise from the irregular surface of a manual contact.

Contributions

Shawn Engell contributed to the conceptualization and design of the study, acquisition of data, analysis and interpretation of data; drafting, revising and approval of the final manuscript.

John J. Triano contributed to the conceptualization and design of the study, acquisition of data, analysis and interpretation of data; drafting, revising and approval of the final manuscript.

James Fox contributed to the conceptualization and design of data analysis, revising and approval of the final manuscript.

Helene Langevin contributed to the conceptualization of the study, analysis and interpretation of data; drafting, revising and approval of the final manuscript.

Elisa Konofagou contributed to the conceptualization and design of acquisition data, analysis and revising and approval of the final manuscript

None of the authors have any conflict of interest. The proprietary software provided by Elisa Konofagu and cited in the manuscript is through Columbia University where she was the scientist engaged in its development.

Conflict of interest

The authors declare that there are no conflicts of interest with respect to the work submitted for publication.

Acknowledgements

The authors would like to acknowledge the financial support of National Center for Complementary and Alternative Medicine of the US National Institutes of Health and the Canadian Institute of Health Research under joint grant number 1R21AT004059-01A1 and of Steve

Tran, MSc and Maricelle Dinulos who assisted in all data collection and pre-processing for analysis.

References

Bereznick, D.E., Ross, J.K., McGill, S.M., 2002. The frictional properties at the thoracic skin-fascia interface: implications in spine manipulation. Clin. Biomech. 17 (4), 297–303.

Brereton, L.C., McGill, S.M., 1998. Frequency response of spine extensors during rapid isometric contractions: effects of muscle length and tension. J. Electromyogr. Kinesiol. 8 (4), 227–232.

Chaffin, D., Andersson, G., 1984. Occupational Biomechanics. John Wiley & Sons, New York, p. 70.

Cleland, J.A., Fritz, J.M., Kulig, K., Davenport, T.E., Eberhart, S., Magel, J., Childs, J.D., 2009. Comparison of the effectiveness of three manual physical therapy techniques in a subgroup of patients with low back pain who satisfy a clinical prediction rule. A randomized clinical trial. Spine 34 (25), 2720–2729.

Colloca, C.J., Keller, T.S., Gunzburg, R., 2003. Neuromechanical characterization of in vivo lumbar spinal manipulation. Part II. Neurophysiological response. J. Manip. Physiol. Ther. 26 (9), 579–591.

Cramer, G.D., Darby, S.A., 2005. Clinical Anatomy of the Spine, Spinal Cord, and ANS. second ed Elsevier, St. Louis, p. 7.

Cramer, G.D., Darby, S.A., 2014. Clinical Anatomy of the Spine, Spinal Cord, and ANS. third ed Elsevier, St. Louis, p. 217.

Descarreaux, M., Dugas, C., 2010. Learning spinal manipulation skills: assessment of biomechanical parameters in a 5-year longitudinal. J. Manip. Physiol. Ther. 33, 226–230.

Descarreaux, M., Dugas, C., Raymond, J., Normand, M.C., 2005. Kinetic analysis of expertise in spinal manipulative therapy using an instrumented manikin. J. Chiropr. Med. 4 (2), 53–60.

Fox, J.R., Gray, W., Koptiuch, C., Badger, G.J., Langevin, H.M., 2014. Anisotropic tissue motion induced by acupuncture needling along intermuscular connective tissue planes. J. Altern. Complement. Med. 20 (4), 290–294.

Gras, L.L., Laporte, S., Mitton, D., Cevier-Denoix, N., Viot, P., 2012. Tensile Tests On A Muscle: Influence of Experimental Conditions and of Velocity on its Passive Response. Proceedings International Research Council on Biomechanical Injuries, Dublin, Ireland (IRC-12-61:515–523).

Huijing, P.A., 2003. Muscular force transmission necessitates a multilevel integrative approach to the analysis of function of skeletal muscle. Exerc. Sport Sci. Rev. 31 (4), 167–175.

Kawchuk, G.N., Perle, S.M., 2009. The relation between the application angle of spinal manipulative therapy (SMT) and resultant vertebral accelerations in an in situ porcine model. Man. Ther. 14 (5), 480–483.

Kawchuk, G.N., Prasad, N., Parent, E., Chapman, S., Custodio, M., Manzon, M., Wiebe, A., Dhillion, S., 2011. Spinal depth landmark in relation to body mass index. Man. Ther. 16 (4), 384–387.

Konofagou, E., Ophir, J., 1998. A new elastography method for estimation and imaging of lateral displacements, lateral strains, corrected axial strains and Poisson's ratios in tissues. Ultrasound Med. Biol. 24 (8), 1183–1199.

Koritke', J.G., Sick, H., 1983. Atlas of Sectional Human Anatomy—Frontal, Sagittal, and Horizontal Planes. Vol. 1. Urban & Schwarzenberg, Baltimore-Munich, pp. 77–91.

Langevin, H.M., Steven-Tuttle, D., Fox, J.R., Badger, G.J., Bouffard, N.A., Krag, M.H., Wu, J., Henry, S.M., 2009. Ultrasound evidence of altered lumbar connective tissue structure in human subjects with chronic low back pain. BMC Musculoskelet. Disord. 3 (10). http://dx.doi.org/10.1186/1471-2474-10-151 151(10).

Langevin, H.M., Fox, J.R., Koptiuch, C., Badger, G.J., Greenan-Naumann, A.C., Bouffard, N.A., Konofagou, E.E., Lee, W.N., Triano, J.J., Henry, S.M., 2011. Reduced thoracolumbar fascia shear strain in human chronic low back pain. BMC Musculoskelet. Disord. 203 (12). http://dx.doi.org/10.1186/1471-2474-12-203.

Maas, H., Sandercock, T.G., 2010. Force transmission between synergistic skeletal muscles through connective tissue linkages. J. Biomed. Biotechnol. http://dx.doi.org/10.1155/2010/575672.

Nash, L.G., Phillips, M.N., Nicholson, H., Barnett, R., Zhang, M., 2004. Skin ligaments: regional distribution and variation in morphology. Clin. Anat. 17 (4), 287–293.

Nathan, M., Keller, T.S., 1994. Measurement and analysis of the in vivo posteroanterior impulse response of the human thoracolumbar spine: a feasibility study. J. Manip. Physiol. Ther. 17 (7), 431–441.

Nougarou, F., Dugas, C., Loranger, M., Page, I., Descarreaux, M., 2014. The role of preload forces in spinal manipulation: experimental investigation of kinematic and electromyographic responses in healthy adults. J. Manip. Physiol. Ther. 37 (5), 287–293.

Ophir, J., Cespedes, I., Ponnekanti, H., Yazdi, Y., Li, X., 1991. Elastography: a quantitative method for imaging the elasticity of biological tissues. Ultrason. Imaging 13 (2), 111–134.

Pickar, J.G., 2002. Neurophysiological effects of spinal manipulation. Spine J. 2, 357–371.

Reed, W.R., Cao, D.Y., Long, C.R., Kawchuk, G.N., Pickar, J.G., 2013. Relationship between biomechanical characteristics of spinal manipulation and neural responses in an animal model: effect of linear control of thrust displacement versus force, thrust amplitude, thrust duration, and thrust rate. Evid. Based Complement. Alternat. Med. http://dx.doi.org/10.1155/2013/492039.

Snodgrass, S.J., Rivett, D.A., Sterling, M., Vicenzino, B., 2014. Dose optimization for spinal treatment effectiveness: a randomized controlled trial investigating the effects of high and low mobilization forces in patients with neck pain. J. Orthop. Sports Phys. Ther. 44 (3), 141–152.

Triano, J.J., Bougie, J., Rogers, C., Scaringe, J., Sorrels, K., Skogsbergh, D., 2004. Procedural skills in spinal manipulation do prerequisites matter? Spine J. 4 (5), 557–563.

Triano, J.J., Gissler, T., Forgie, M., Milwid, D., 2011. Maturation in rate of high-velocity, low-amplitude force development. J. Manip. Physiol. Ther. 34 (3), 173–180.

Triano, J.J., Descarreaux, M., Dugas, C., 2012. Biomechanics—review of approaches for performance training in spinal manipulation. J. Electromyogr. Kinesiol. 22 (5), 732–739.

Triano, J., Giuliano, D., McGregor, M., Howard, L., 2014. Enhanced Learning of Manipulation Techniques Using Force-Sensing Table Technology (FSTT). Higher Education Quality Council of Ontario, Toronto.

Triano, J.J., Giuliano, D., Kanga, I., Starmer, D., Brazeau, J., Screaton, C.E., Semple, C., 2015. Consistency and malleability of manipulation performance in experienced clinicians. J. Manip. Physiol. Ther. http://dx.doi.org/10.1016/j.jmpt.2015.05.002.

Yucesoy, C.A., 2010. Epimuscular myofascial force transmission implies novel principles for muscular mechanics. Exerc. Sport Sci. Rev. 38 (3), 128–134.